# **Author's Personal Copy**

Journal of Manufacturing Processes 54 (2020) 251-261

ELSEVIER

Contents lists available at ScienceDirect

## Journal of Manufacturing Processes

journal homepage: www.elsevier.com/locate/manpro



# Understanding process force transients with application towards defect detection during friction stir welding of aluminum alloys



Daniel Franke, Shiva Rudraraju, Michael Zinn, Frank E. Pfefferkorn\*

Department of Mechanical Engineering, University of Wisconsin-Madison, Madison, WI, USA

ARTICLE INFO

Keywords:
Friction stir welding
Aluminum
Defect
Process monitoring
Forces

#### ABSTRACT

The formation of sub-surface defects during friction stir welding has limited the adoption of the process in high volume production. A potential exists to eliminate/reduce the need for costly post weld inspection of such defects through the development of an in-process defect detection method based on a measured process output. The current state of in-process defect detection consists primarily of applying "black box" methods of correlating process outputs to defect occurrence without a fundamental physical understanding of what is producing the change in the output. This approach constrains the application of such methods when altering any aspect of the friction stir welding process. The current study seeks to provide a fundamental physical explanation as to what is driving the oscillation of friction stir welding process forces at the tool rotational frequency, as well as what is occurring when the tool interacts with defects and the oscillatory process forces are altered. A novel understanding was enabled through the synchronization of force measurements with angular position measurements of tool features. The results suggest that the eccentric motion of the tool and/or the rotation of a slanted shoulder surface are the primary drivers of process force oscillations. A fundamental explanation of the interaction between features on the tool probe and defective volumes has been proposed. The physical understanding helps to explain how altering the process will alter the force transients on which the detection method is based, which will enable a more robust and transferable method.

## 1. Introduction

The friction stir welding (FSW) process (Fig. 1) consists of plunging a rotating non-consumable tool into two metallic workpieces and traversing the tool along a joint line in order to mechanically intermix the two workpieces [1]. The plastic deformation of the workpieces generates heat which produces temperatures on the order of 80–95 % of the solidus temperature of the alloy. The elevated temperature is instrumental in facilitating plastic deformation of the workpieces, but with the key aspect that the process does not melt the material. The solidstate nature of the process provides distinct advantages over fusion based welding processes. These advantages include a less severe heat affected zone, minimal distortion and residual stresses, avoidance of hot cracking, reduction/elimination of shielding gas, energy efficiency, and grain refinement within the stir zone due to dynamic recrystallization. A significant amount of research has shown that FSW can be used as an energy-efficient method of creating high-quality joints in lightweight alloys such as aluminum and magnesium [2,3].

However, friction stir welding does possess limitations. Currently, the process is limited in terms of travel speed, which has hindered its

adoption in high volume production settings. An increase in travel speed is more likely to result in an inadequate thermomechanical state that prevents the material from being successfully deformed around the tool and deposited in the weld. The breakdown in material flow results in volumetric defects within the weld that are detrimental to joint performance. Defects tend to form in the probe driven region of the weld resulting in sub-surface defects that cannot be detected visually. The sub-surface nature requires a post-process non-destructive evaluation technique (e.g. ultrasonic testing [4,5], eddy current testing [6,7]) to determine if the weld is compromised. In many cases, the additional step of applying a post process non-destructive evaluation technique is cost-prohibitive. The development of a robust in situ defect detection method based on a measured process output has the potential to address this limitation. The goal of this work is to both further the fundamental understanding of how sub-surface defects are formed as well as advance the development of a force measurement based defect detection method.

E-mail address: frank.pfefferkorn@wisc.edu (F.E. Pfefferkorn).

<sup>\*</sup> Corresponding author.

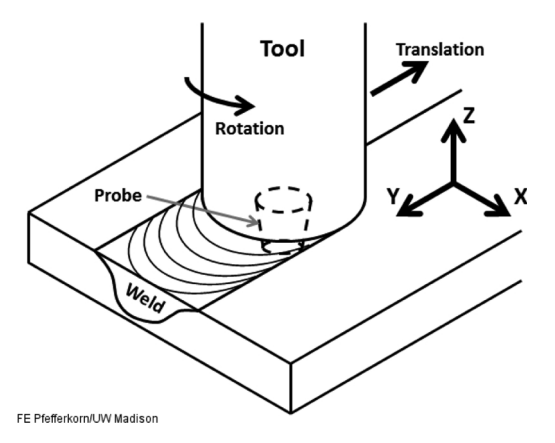
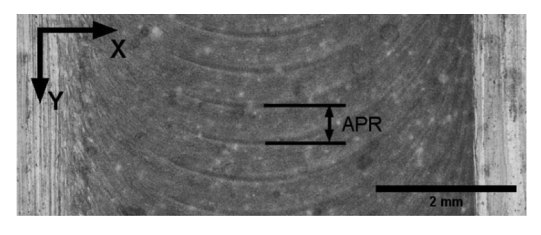


Fig. 1. Schematic of the friction stir welding process defining the 3-axis coordinate system referred to in this study.

### 1.1. Intermittent material flow during friction stir welding

One feature often observed in the microstructure of most friction stir welds is the layers (or bands) of material that form in the cross sections of welds in the plane of welding (X-Y plane in Fig. 1). The banded features, which form at the distance that the tool advances in one revolution (Fig. 2), are resultant of material flow around the tool probe in an intermittent manner at the period of one revolution. The mechanisms driving this intermittent flow are not completely understood. Some researchers have proposed that it stems from a change in contact condition (sticking vs. sliding) between the material and the tool [8,9]. Abergast [10] initiated a hypothesis, which was later articulated by Boldsaikhan et al. [11], involving the opening and filling of a cavity once per revolution in the wake of the tool probe. Nunes [12] proposed that strain localization propagates a batch-wise flow of material around the tool similar to the shear banding process observed in machining chips. Fonda et al. [13], measured a change in shear textures within a single band which led the researchers to propose that the banded nature comes from an oscillatory motion (precession) of the tool due to the natural eccentricity (i.e., tool runout) as well as an oscillatory deflection of the tool due to the oscillation in process forces during friction stir welding. Gratecap et al. [14], tested tools with different levels of eccentricity (runout) and showed that tools with larger runout moved more material around the tool per revolution, leading the researchers to propose that the banded structure stems primarily from tool runout. Reynolds [15] proposed that even small amounts of tool runout can create differences in strain rates that produce the change in microstructure seen once per revolution. Chen et al. [16], proposed that each band is formed by the threads on a threaded tool probe. It is also possible that the banded structure is formed through a combination of several of the previously listed hypothesis, i.e., tool runout could initiate strain localization and/or an opening and closing of a cavity in the wake of the tool probe. A fundamental understanding of the intermittent nature of material flow is important because significant research has shown that a breakdown in the intermittent flow of material around the probe is what commonly leads to sub-surface defects within



**Fig. 2.** Reflected white light image of mid-plane cross section of a weld (2.5 mm below surface) showing the banded microstructure formed at the advance per revolution (APR).

friction stir welds in aluminum alloys [11, 17, and 18].

## 1.2. Oscillatory component of process forces

Significant research has shown that the process forces during friction stir welding tend to oscillate at the tool rotational frequency [11,15–25,33–36]. Since the intermittent flow of material occurs once per tool revolution, and the process forces oscillate once per tool revolution, researchers have concluded that the two are fundamentally linked [11,15-18,22,23,33,34]. Either the intermittent movement of material initiates the application of the oscillatory component of the force onto the tool, or the eccentric motion of the tool initiates the application of the force onto the material. Boldsaikhan et al. [23], developed a two-dimensional model that involved a prevailing pressure field due to the translation of the tool and a revolving pressure field due to the intermittent shear layer. This model was based on the concept that the formation of the shear layer initiates the force onto the tool. Other researchers have suggested that the eccentric nature of the tool (i.e., runout) generates the oscillatory component of the forces [15,22,24,25]. Zaeh et al. [24], have shown that for two different tool setups with different amounts of runout, the greater runout results in a significantly larger amplitude of the oscillating component of the forces. In addition, both Zaeh et al. [24], and Panzer et al. [25], have proposed that the oscillating components of the process forces are affected by the complex dynamics of the machine and that modeling the whole machine/process system is critical to the modeling of the process forces.

## 1.3. Force and torque based defect monitoring

Assuming that the oscillatory nature of the process forces is directly related to the flow of material around the friction stir tool probe once per tool revolution, then a breakdown in the material flow should produce a change in the measured force oscillation. If a change in force can be captured during welding and correlated to the presence of volumetric defects within the weld, then the need for post-weld inspection can be reduced/eliminated. Mishra et al. [26], have prepared a review on in-process monitoring and control of the friction stir welding process. Force and torque measurements are the most commonly studied process outputs since they tend to have better sensitivity and/or respond faster to defect occurrence than other process outputs such as temperatures, electrical power, electrical current, vibrations, and acoustic emissions. Several different methods of force and torque-based monitoring have been discussed in the literature [27-33]. The focus of the current work is not to develop a full monitoring method, but rather explain the physics underlying certain force transients that could be used to form the basis of a force-based monitoring system. Because of this, the details of the prior methods are not elaborated on in this manuscript. A more detailed description of prior force and torque-based methods can be found in Mishra et al. [26] or in Shrivastava et al. [18]. One important conclusion that can be drawn from the prior literature is that, in general, a significant limitation in prior studies is that they do not provide fundamental explanations as to what is physically occurring that produces the changes in process forces or torques when defects are forming. They often apply a "black box" approach of correlating inputs (feedback forces/torques) to outputs (defect occurrence). This limits the method when altering any aspect of the friction stir welding process because it is difficult to know when and how a "black box" correlation approach will translate. It is not even known if a method that was developed based on data from 6061-T6 aluminum welds can be applied to a different aluminum alloy. A fundamental understanding of what is physically occurring is crucial to developing a robust method that can be generalized and applied more broadly without limiting it to a specific machine, tool, weld configuration, workpiece alloy, and parameter space combination.

The current work is a continuation of the research performed by

Shrivastava et al. [18,34], which provided evidence that defects created with tools consisting of various numbers of flats on the tool probe can distort the oscillating component of the force signal. The distortion generated an amplitude in the force signals at the frequency equal to the tool rotational frequency multiplied by the number of flats (harmonics of the rotational frequency). In [18], the researchers used a tool with a three flat probe and quantified the amplitude of the force signal at the third harmonic of the tool rotational frequency using a discrete Fourier transform. The amplitude of the third harmonic was used to develop a correlation between the process forces and the volume of defects within welds (measured through X-ray imaging). The physical explanation of the force oscillation at the tool rotational frequency is described as a cavity opening and filling in the wake of the tool. The explanation of the third harmonic is stated as an interaction between the flats on the tool probe and the voided region. However, a detailed physical description of said interaction is not provided. The focus of the current work is to provide a fundamental explanation of what is physically occurring in terms of the interaction between the tool and workpiece at both the tool rotational frequency and the third harmonic. This fundamental understanding is critical to expanding the method to different tool geometries, friction stir welding machines, and workpiece alloys.

#### 2. Methods

### 2.1. Experimental apparatus

Friction stir welding was performed on a 3-Axis CNC Mill (HAAS, TM-1). A magnetic angular encoder (HAAS, Part #: 30-30390, 1024 pulses per revolution) mounted on the top of the spindle was used to measure the angular position of the friction stir tool during welding. Differential signals from the magnetic encoder were fed to an optical isolator (AutomationDirect, FC-ISO-C) for noise rejection. The optical isolator serves to isolate the electrical grounds between the data acquisition system and the CNC mill, as well as convert the differential encoder signals to single ended signals. Workpieces were mounted on a three-axis piezoelectric force dynamometer (Kistler, model 9265). Charge signals from the dynamometer were fed to charge amplifiers. Outputs from the optical isolator and charge amplifiers were connected to the data acquisition system (National Instruments, BNC-2090A, PCI-6014, PCIe-6320). The system provided the ability to measure the net forces that the friction stir tool applies to the workpiece (in the X, Y, and Z directions in Fig. 1) in conjunction with the angular position of the friction stir tool. This provided the capability of resolving the angular position of features on the tool (e.g., flats, eccentric points) at a given point in time with measured force values. The data acquisition system was triggered to sample the force signals at every pulse of the encoder, which produces 1024 data points per revolution. A full schematic of the data acquisition system can be found in the Supplementary Material (Section 1).

## 2.2. Friction stir tools

Three friction stir (FS) tools, manufactured by Friction Stir Link Inc. out of H13 tool steel and coated in their proprietary "Alpha Coating," were utilized. The specific geometry of the tools was developed by Friction Stir Link Inc. in the early 2000s, through industrial application of the tools in aluminum alloys. The tools were chosen because they are similar to the tools used in the prior studies of similar force transients [18,34]. All three tools were nominally the same, consisting of a 15 mm diameter concave shoulder and a 5.1 mm long probe that tapered from 7 mm at the shoulder down to 5 mm at the tip. The probe of each tool had three flats spaced 120 deg. apart. All flats had a constant depth of 0.625 mm from the outer diameter of the probe. The probe was also threaded with a 1 mm pitch and a constant thread depth of 0.625 mm. There are two bulk geometric imperfections in the friction stir tools that

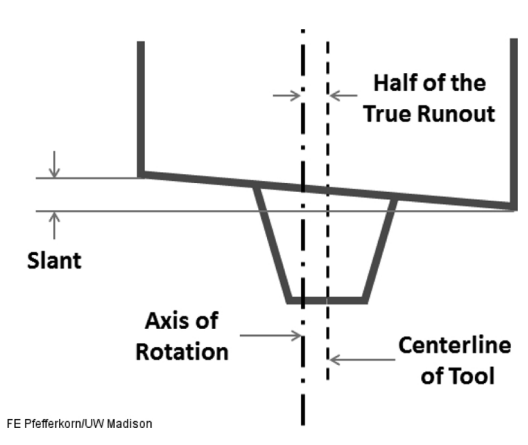


**Fig. 3.** Schematic of the two primary tool imperfections that drive process force oscillations

were examined in this study (Fig. 3). When the tools were mounted in the spindle, each tool had some degree of natural runout (eccentricity from the true rotational axis) as well as a slant in the tool shoulder (tool shoulder that is not level with respect to the true rotational axis of the machine). The term "slant" does not refer to the travel angle of the tool that is commonly used in friction stir welding. It is a slant in the tool shoulder that rotates with the tool. The runout and slant of each tool (as it rotates in the machine spindle) were measured kinematically at the edge of the tool shoulder on each corresponding face by means of fixing a dial indicator to the mill table, loading the indicator against the surface of the tool, and rotating the tool freely in the spindle. The dial indicator had a resolution of  $2.5 \, \mu m$  (ten-thousandths of an inch). The angular position of the most eccentric part of the tool and the lowest part of the slanted shoulder (the part that will dig deepest into the material) were marked on all of the tools. The values of true runout (double the value depicted in Fig. 3) and tool slant for all three tools are listed in Table 1.

The slant and runout of each tool are a product of how the tools are manufactured and mounted in the tool holder (an image of the tool holder setup is contained in the Supplementary Material: Section 2). The FS tools are machined in two steps. First, the workpiece side (consisting of the probe and shoulder) was turned, and the probe flats are milled. Next, the tool was unclamped and rotated 180 degrees so that the threads by which the tool is threaded into the tool holder adaptor can be machined. The inherent mismatch between the two machining setups is one significant contributor to the tool imperfections. The other important contribution comes from the mating of the tool holder adaptor with the set screws that hold it in the standard CAT 40 tool holder utilized. The most eccentric point on the tool will tend to be opposite the set screws. It is assumed that the two measurements described in this section accurately capture the bulk of the geometric imperfections of the tool given the nature of the tool holder setup, and considering that the shoulder and probe are turned together in the same machining step.

## 2.3. Experimental procedure

All welds were performed as bead-on-plate welds in aluminum 6061-T6 workpieces that were 203 mm (8 in.) long, 102 mm (4 in.)

 Table 1

 Values of measured true runout and shoulder slant for each tool.

	Tool 1	Tool 2	Tool 3
Runout	46 μm (0.0018 in)	74 µm (0.0029 in)	183 μm (0.0072 in)
Slant	10 μm (0.0004 in)	5 μm (0.0002 in)	15 μm (0.0006 in)

wide, and 6.35 mm (0.25 in.) thick. All welds were performed at a length of 150 mm, at a 3-degree travel angle, and with a backing plate made of 6.35 mm thick mild steel. To set the reference point for the tool plunge depth, a preload of 20 N was applied to a precision ground gage block placed at the trailing edge of the tool shoulder. All welds were performed with a commanded shoulder plunge depth of 0.2 mm at the center of the tool. However, the machine compliance in the axial (Z) direction (approximately 0.05 mm/kN [37]) results in the center of the tool shoulder residing at approximately the top surface of the workpiece during welding. Prior to starting the data acquisition system, a reference point for the tool's angular position data was set by positioning one of the tool probe flats against the front face of the workpiece fixture (perpendicular to the weld direction).

#### 2.3.1. Effect of tool runout and shoulder slant on oscillatory process forces

To examine the effect tool runout and slant on the oscillatory component of the process forces, welds were first performed with the tools in their baseline state as described in Table 1. Two welds were performed for each tool at 1000 rpm and 200 mm/min. Subsequently, the slant in the tool shoulder with respect to the true rotational axis of the tool was eliminated by fixing a turning tool to the table of the CNC mill used for friction stir welding, and turning the shoulders of each of the tools to make them level with respect to the true rotational axis of the tool as it spins in the milling machine spindle. The slant in all tools after machining was less than the resolution of the dial indicator (2.5 μm), leaving only a significant runout of the tools. After leveling the tool shoulder with the rotational axis of the tool, the same welds were performed at 1000 rpm and 200 mm/min with two replications for each tool. Post welding, a discrete Fourier transform was used to extract the amplitude of the oscillating component of the force signals in the X and Y directions over a period of 20 tool rotations once a steady-state condition, in terms of process forces, had been reached at approximately100 mm into the weld length.

## 2.3.2. Effect of tool runout on defect formation

To examine the effect of tool runout on defect formation and force-based defect detection, welds were performed at increasing amounts of advance per revolution (APR) to create welds without defects at low advance per revolution and welds with defects at higher advance per revolution. Welds were performed at three rotational rates: 800, 1000, and 1200 rpm. The travel speed was then set to produce welds with advance per revolutions ranging from 0.3 to 0.8 mm/rev for each spindle speed. The full range of welding parameters that each individual tool was tested at is shown in Table 2. For Tool 3 (183 µm runout), the highest three advance per revolution conditions were not performed since this particular tool started to form defects at lower travel speeds than Tools 1 and 2. A total of 54 welds were performed.

Post welding, three cross sections (each 15 mm apart) were cut from each weld (in the X-Z plane in Fig. 1) at a distance approximately halfway along the weld to ensure the weld had reached a steady state condition in terms of process forces. All cross sections were mounted, ground, and polished in order to expose the presence of sub-surface defects. Images of all defects were capture using white light optical microscopy (Alicona Infinite Focus). The areas of the defects within each cross section were determined

 Table 2

 Parameters used to create defective and non-defective welds for all three tools.

APR	800 rpm	1000 rpm	1200 rpm
0.3 mm	240 mm/min	300 mm/min	360 mm/min
0.4 mm	320 mm/min	400 mm/min	480 mm/min
0.5 mm	400 mm/min	500 mm/min	600 mm/min
0.6 mm	480 mm/min	600 mm/min	720 mm/min
0.7 mm	560 mm/min	700 mm/min	840 mm/min
0.75 mm	600 mm/min	750 mm/min	900 mm/min
0.8 mm	640 mm/min	800 mm/min	960 mm/min

using an image analysis method developed in Mathworks MATLAB. The images were converted to black and white, where the aluminum becomes white (pixel values close to 255) and the defects become black (pixel values less than 100). A threshold value of 250 was set for segmenting all images. The images were then cleaned so that all artifacts smaller than 5 pixels in diameter are converted to the surrounding medium. An example of the segmentation process along with a sample histogram of the image is contained in the Supplementary Material: Section 3. The number of defect pixels was then counted and converted to an area value using the number of pixels in the scale bar outputted from the microscope software.

#### 3. Results and discussion

## 3.1. Explanation of oscillatory process forces

The fundamental basis of the current defect detection method is that the oscillatory process forces are linked to the intermittent flow of material around the tool probe, and that a breakdown in material alters the force oscillation. Therefore, the development of this method requires a fundamental understanding of the mechanisms driving the oscillation. It was hypothesized that the geometric imperfections in the friction stir tool depicted in Fig. 3 drive the oscillation. This hypothesis was examined by comparing the direction of the resultant component of the oscillatory process force in the plane of welding (X-Y plane) to the angular position of features on the FS tool (enabled through the encoder data). The focus of the analysis is to isolate the direction of the oscillating part of the process forces (i.e., the components of the force signals that rotate with the tool) in the X-Y plane. The process of deriving the direction of the resultant force from the measured X and Y force signals is described in the following text and illustrated in Figs. 4 and 5. During welding, the tool will apply an average force to the workpiece in the direction of travel (as shown in Figs. 4(a) and 5) around which the force oscillates. There is also an average force applied to the workpiece in the X-direction towards the retreating side of the weld around which the force oscillates. It is hypothesized that the average force in the X-direction is due to stronger shearing in front of the tool as compared to in the wake of the tool. Since the goal is to examine the direction of the force oscillation in the X-Y plane, both of the average forces are removed (signals normalized) before the resultant force is calculated in order to isolate the direction of the oscillatory component itself. The compass plots shown throughout this manuscript are the result of taking the measured force signals in the X and Y directions, eliminating the average components of the force signal (Fig. 4(b) and (c)), then combining the normalized X and Y force values at a singular point in time to form a resultant force in the X-Y plane (Fig. 4(d)). The arrow in the compass plot shows the direction and amplitude of the oscillatory component of the force that the tool is applying to the workpiece material. The angular position of the features on the tool probe at the given time when the resultant force is calculated can be overlaid on the compass plot since the angular encoder pulses were used to trigger the force measurements. This process will result in a depiction of the direction of the oscillatory force relative to the angular positions of features

The direction and amplitude of the resultant force during the steady-state of a representative non-defective weld for each of the three tools prior to leveling the tool shoulder with the CNC mill is illustrated in Fig. 6. All plots are shown for an arbitrary given point in time when the reference flat, used to zero the encoder data, is at the trailing edge of the tool. The angular positions of the tool features at this specific point in time are overlaid on the compass plot. The tool is represented as a cross-section of the probe in the X-Y plane showing the angular location of the three flats. The dashed line labeled "RO" represents the angular position of the most eccentric point of the tool runout and the dashed and dotted line labeled "S" represents the angular position of the lowest point of the slanted tool shoulder. The dashed circle represents the tool path for the eccentric rotation of the tool. Note that the eccentric tool path is not to scale. For Tools 1 and 2 (lower tool runout) the direction of the resultant force is close to perpendicular to the angular position of the low point in the tool shoulder slant and leads the slant in the

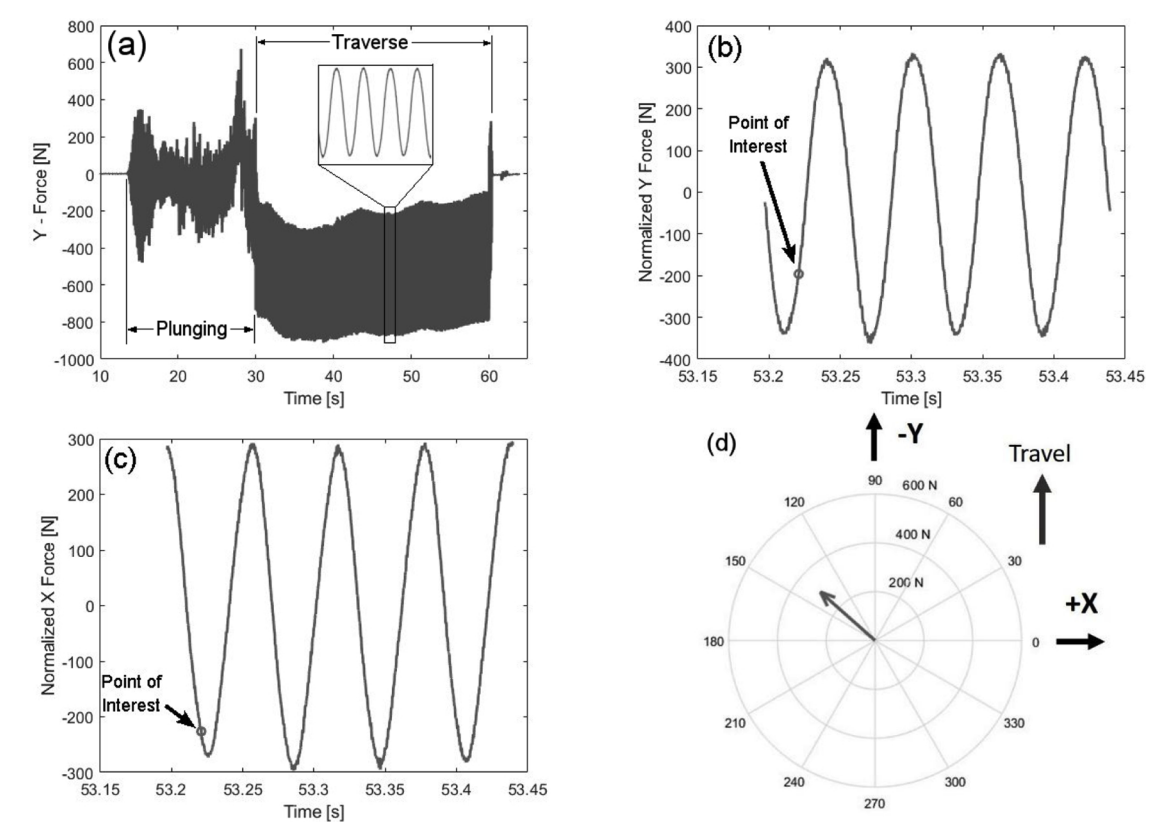
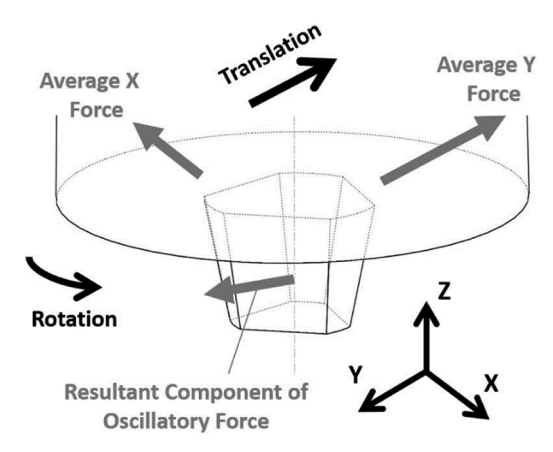


Fig. 4. Generation of the resultant direction of the oscillatory component of the process forces in the X-Y plane: (a) the full measured Y force signal, (b) the normalized Y force with selected value at time of interest, and (d) combination of selected X and Y force at time of interest in the plane of welding.



**Fig. 5.** Schematic of the three force vectors derived from the X and Y force signals. At a given point in time, the addition of all three vectors describe the total force the tool applies to the workpiece in the X-Y plane. Note that the direction of the resultant force will rotate with the tool and is shown in an arbitrary position in this figure.

direction of rotation (counterclockwise). This suggests that as the tool rotated, the low point of the shoulder that dug deepest into the workpiece material applied a force to the workpiece in the direction of rotation. In contrast, for Tool 3, the large amount of runout appears to outweigh the effect of the shoulder slant and forces the direction of the resultant force to be towards the most eccentric part of the tool. This suggests that the eccentric motion of the tool probe applies a normal force to the workpiece material as it rotates.

Looking closer at Tools 1 and 2, it appears that the angle between the direction of the resultant force and the low point of the slanted shoulder is closer to  $90^\circ$  for Tool 1 than for Tool 2. It is hypothesized that this occurs because the runout of Tool 1 is smaller than that of Tool 2, and Tool 1 has slightly more slant than Tool 2. When examining Tool 2, the direction of the resultant force is slightly less than  $90^\circ$  from the low slant position (towards RO position) because there is some contribution from the larger runout of Tool 2, and slightly less slant of the shoulder (5  $\mu m$ ) compared to Tool 1 (10  $\mu m$ ). It can be concluded that the direction of the resultant force is driven by a combination of the two geometric imperfections based on the magnitude of each. This suggest that specific alignment of the angular positions of the slant and runout causes them to add together (runout leads slant) or subtract from each other (runout trails slant).

The directions of the resultant forces with respect to the features shown in this section were confirmed by performing multiple repetitions of each weld. Within a complete rotation, the direction of the force with respect to the angular position of the tool remains constant, *i.e.*, there is no significant change in phase between the direction of the force and angular position of the tool within one rotation. This is illustrated in Fig. 7, which shows the resultant force in increments of 120° of tool rotation. It can also be observed that the amplitude of oscillation is slightly larger in the direction of travel (Y-direction) than in the direction perpendicular to travel. This results in an elongated ellipse in the direction of travel when plotting the full polar plot of the resultant force for one full revolution, as shown in Fig. 7(d). It is hypothesized that this elongation occurs because the eccentric motion is superimposed upon the travel motion.

The directions of the resultant force with respect to tool features

D. Franke, et al.

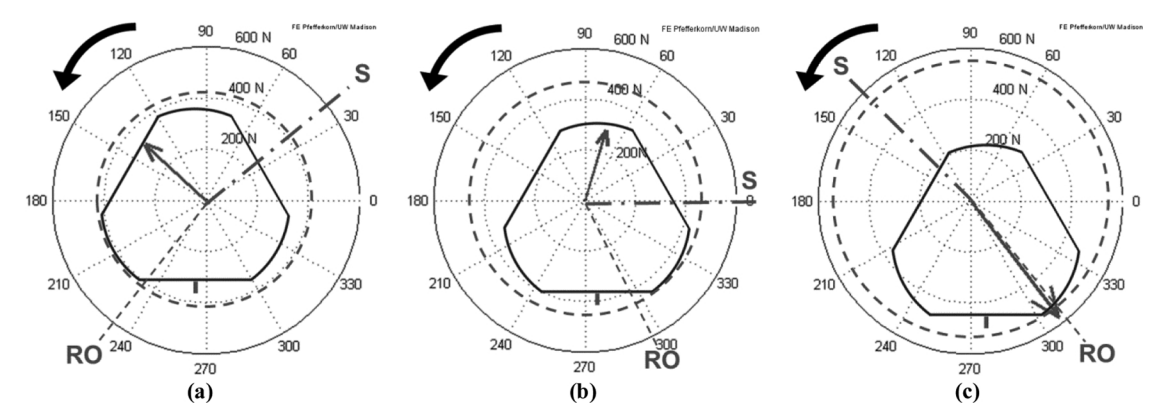


Fig. 6. Direction of resultant force with respect to angular position of tool features prior to leveling of tool shoulder for (a) Tool 1, (b) Tool 2, and (c) Tool 3. Note: The circle representing eccentric tool path is not to scale.

after the shoulders of each tool had been machined level with the true rotational axis of the tool are shown in Fig. 8. Without the low point of the tool shoulder digging into the material, only the eccentric motion of the tool probe can apply a significant oscillatory force to the surrounding material. This can be observed for Tools 1 and 2 where the direction of the resultant force now points towards the peak of the tool probe that is nearest the most eccentric angular position of the tool: as opposed to leading the low point in the slanted shoulder as shown in Fig. 6. Additionally, for all three tools, the amplitudes of the oscillatory forces (magnitude of vector) reduced after leveling the tool shoulder. This is seen more clearly in Tool 1 and 2 as the amplitude was first driven by the shoulder slant (before leveling), which was larger than the force applied by the eccentric probe. With the slant removed, the smaller force applied by the eccentric probe manifests itself. The imperfection (slant or runout) that will drive the force oscillation will be dependent on the magnitude of each, as well as the size of the shoulder compared to the size of the probe.

The amplitude of the force oscillations in the X and Y directions for two replications of welds performed at 1000 rpm and 200 mm/min (non-defective) are plotted against the magnitude of the measured kinematic runout of the tool used to perform the weld in Fig. 9. The amplitudes of the force oscillations appear to increase linearly with the measured kinematic runout. The linear relationships have Y-intercept values close to zero newtons of amplitude at a runout value of zero. This suggests that the majority of the force oscillation is driven by the eccentric motion of the tool applying a force to the material around it, *i.e.* there is not an apparent additional mechanism that generates a significant component of the amplitude. These results support the findings reported by Zaeh *et al.* [24] that examined the amplitude of the oscillating process forces for two different tools, one that had a runout of 300  $\mu$ m, and one that had a runout of 1  $\mu$ m, which was created by

turning the tool on the same machine that welding was performed on. Plunging tests (friction stir spot welds) resulted in amplitudes of approximately 300 N and 10 N, respectively, which corroborates the current linear relationships seen. Since it appears that the eccentric motion of the tool is fundamental in generating the oscillatory nature of the process forces, it must be considered when developing a force-based detection method that relies on the oscillatory forces. In addition, the slant of the tool shoulder must be considered if it is a significant factor.

The results contained in this section are fundamental in understanding the underlying mechanisms of material flow during friction stir welding. The observation that the resultant component of the oscillatory process force points toward the most eccentric point of the tool (or leads the low point of a slanted shoulder), in combination with the linear scaling of the amplitude with increased runout suggests, that these imperfections are the primary drivers of the oscillatory process forces. This also suggests that the eccentric motion of the tool probe is the primary driver of the intermittent flow of material around the tool probe. It appears that the oscillatory process forces do not stem primarily from mechanisms previously proposed in literature such as a change in contact condition between sticking and slipping, or from a forming and filling of a cavity once per tool revolution. However, it must be noted that other mechanisms can be present but secondary to the eccentric motion of the tool (for the current welding conditions). It is feasible that the eccentric motion of the tool instigates either strain localization or the opening of a small cavity that then develops into the banded features observed in the microstructure of friction stir welds.

The direction of the resultant force suggests that the equal and opposite reactionary force that the workpiece material applies to the tool should constrain the eccentric motion of the tool. This result contradicts the hypothesis proposed by Fonda et al. [13], which suggested that the oscillatory force helps generate an additional oscillatory

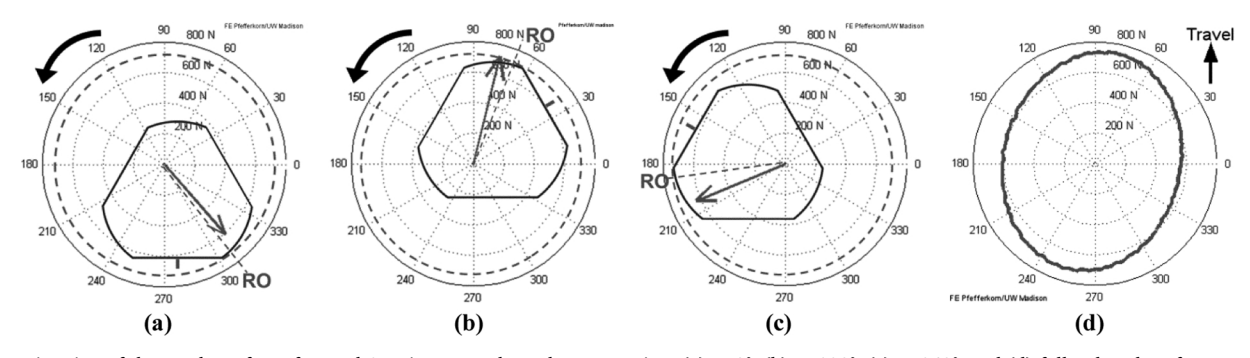


Fig. 7. Direction of the resultant force for Tool 3 as it rotates through one rotation: (a) at 0°, (b) at 120°, (c) at 240°, and (d) full polar plot of one rotation.

D. Franke, et al.

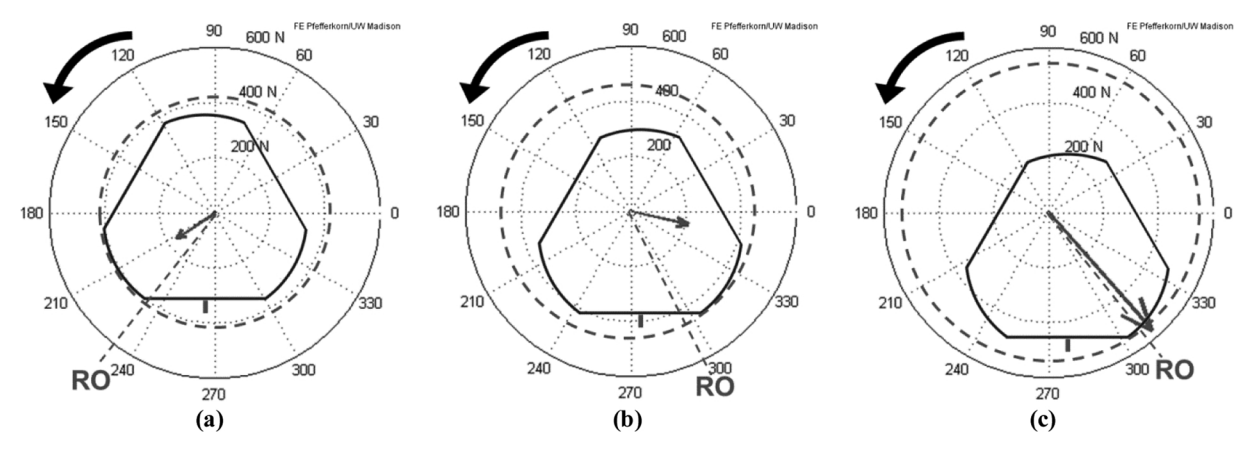
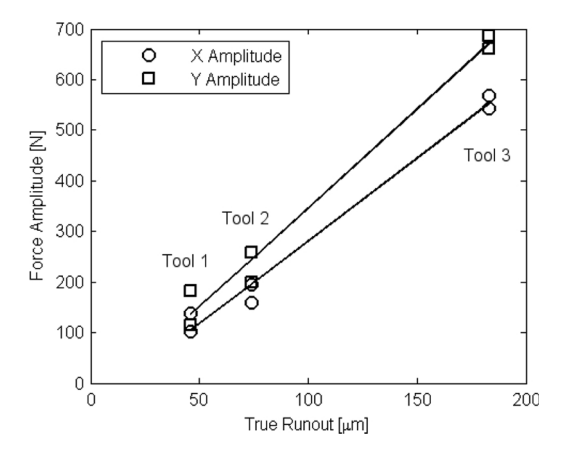


Fig. 8. Direction of resultant force with respect to angular position of tool features after leveling of tool shoulder: (a) Tool 1, (b) Tool 2, and (c) Tool 3.



**Fig. 9.** Relationship between the magnitude of kinematic runout of the tools and the amplitudes of the process force oscillations during good welding conditions.

motion of the tool on top of the tool's natural runout. However, this constraining force observed may only be present in the particular welding conditions studied. A different workpiece alloy and/or a machine with different dynamics has potential to lead to the propagation of the eccentric motion of the tool. Prior research has shown that FSW systems can become unstable, and that a larger oscillatory motion, *i.e.*, long-range oscillation, can be imposed upon the tool [38]. Long-range oscillations due to an instability in machine dynamics (natural frequency, controller instability) should be considered when developing a defect detection method based on oscillatory force transients. *In situ* measurement of the eccentric motion of the tool during welding is the objective of further study by means of laser vibrometry.

## 3.2. Explanation of defect and probe interaction

The core of developing a force-based detection method is the fundamental understanding of the interaction between the tool and workpiece that produces the change in the measured forces. It has previously been determined that features on the tool probe (e.g., flats) can distort the oscillatory process forces at a harmonic frequency corresponding to the number of features [18,34]. This study seeks to provide an explanation as to what occurs physically within the system that produces the amplitudes at the higher harmonics. The explanation is provided through the examination of the resultant force in the X-Y

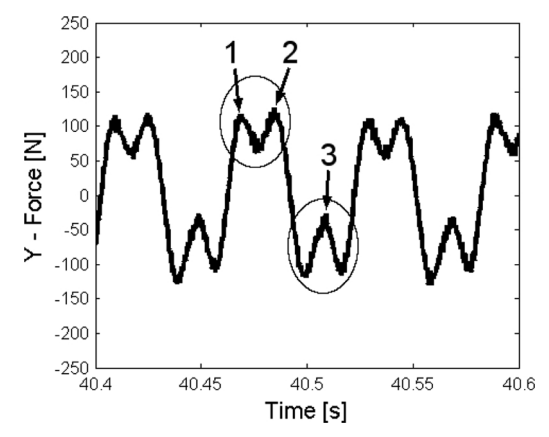


Fig. 10. Distorted force signal for a defective weld. The two interactions per revolution are circled and the three peaks generated are labeled.

plane within one revolution of the tool during a defective weld. There are two distortions that occur in the force signal per revolution that generate an amplitude at the third harmonic (three peaks per revolution) in both the X and Y force signals when using a three-flat tool. The two distortions (circled in Fig. 10) result from momentary reductions in the amplitude of the signal at the primary tool frequency. The reduction in the amplitude appears to be due to a lack of contact between the most eccentric peak of the tool probe (drives force oscillation as shown in the previous section) and the surrounding material due to the absence of material (void). The physical description of how this process occurs within one revolution is explained in further detail in this section.

The progression of the resultant force within one rotation of the tool during a defect interaction is illustrated in Fig. 11, which shows the direction and amplitude of the resultant force in 30° increments for a weld performed with Tool 3 at a rotational rate of 1000 rpm and a travel speed 600 mm/min. Note that the images in Fig. 11 show measured force and angular position of tool features, but only hypothesized deflection of the tool from its eccentric motion (not to scale) and hypothesized void size and location (not to scale). The final location and size of a representative defect formed during this specific weld can be observed in the cross-section shown in Fig. 12. Welds performed with Tool 3 in a good welding condition have an oscillatory force amplitude on the order of 600 N. Therefore, during a good weld, the magnitude of the resultant force remained a relatively consistent 600 N throughout

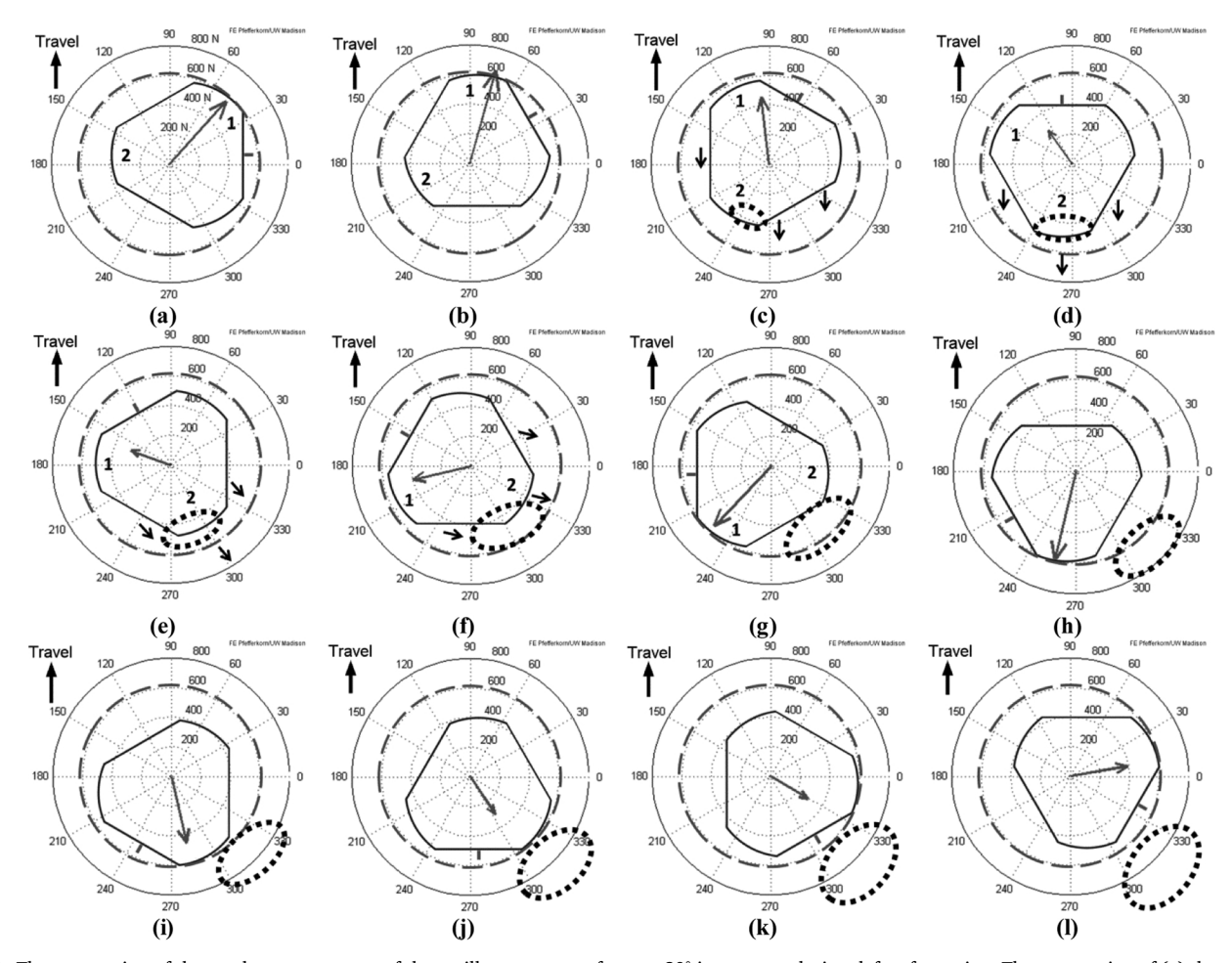
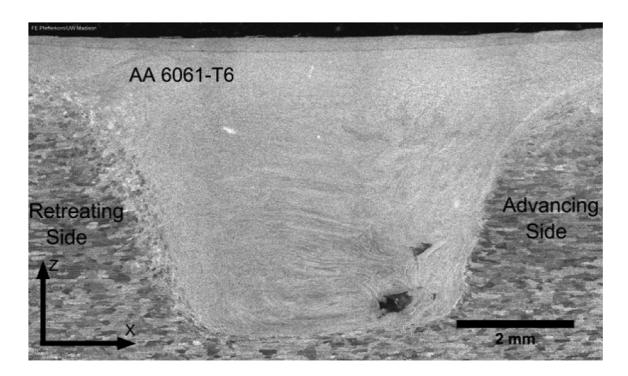


Fig. 11. The progression of the resultant component of the oscillatory process force at 30° increments during defect formation. The progression of (a) through (l) is described in the proceeding text. Note: the force and angular positions are measured but the size and location of tool deflection and voided region are hypothesized and not to scale.



**Fig. 12.** Size and location of the defect within the weld that is represented by the force data in Fig. 11.

the rotation, and its direction followed the most eccentric peak of the tool probe (Fig. 7). However, when a defect is formed, the resultant force will be altered in the manner as described for each of the corresponding figure letters (Fig. 11) as follows:

- a) The most eccentric peak (Peak 1) is in the upper right quadrant causing the resultant force to point toward that peak with an amplitude of approximately 600 N, which is indicative of full contact between that peak and surrounding workpiece material.
- b) The existing condition is similar to the condition described in (a). In addition, note that the majority of the material that is moved per revolution is opposite the most eccentric peak of the tool and now

- resides at the trailing edge of the tool, *i.e.*, the majority of the material is now being extruded in the wake of the tool which is when a breakdown in flow resulting in a defect is most likely to manifest itself due to the intermittent nature of the flow.
- c) A lack of material flow into the wake of the tool due to an inadequate thermomechanical state results in the formation of a void
  volume. The void volume is represented by the dark dotted circle.
  Currently, the void is located where the peak of the tool probe
  leading the most eccentric peak (Peak 2) is located. It is hypothesized that at this point the entire tool starts to deflect back into this
  voided region since less material is present to constrain the tool. The
  deflection is driven by the large average force being applied to the
  tool by the material ahead of the tool as the tool travels. This small
  amount of deflection (represented by the small arrows) results in a
  reduction in pressure at the leading edge of the tool where Peak 1
  resides, which is why the magnitude of the resultant force at the
  leading edge has started to drop to near 400 N.
- d) As the void region continues to expand due to a lack of flow around the tool probe, the tool continues to be deflected back into the void region causing a further reduction in the magnitude of the resultant force at the leading edge, which is now approximately 300 N.
- e) The tool is still deflected into the void region by the average forces resulting in the reduced magnitude of the resultant force.
- f) Peak 2 is now starting to leave the void region and contact solid material on the advancing side of the weld. This contact will now prevent deflection, and thus the magnitude of the resultant force will start to increase.

- g) Peak 2 has now moved out of the voided region and is contacting solid material on the advancing side of the weld. This prevents the tool from defecting from its original path and restores the magnitude of the force that the eccentric tool applies to the workpiece (back to 600 N).
- h) Neither peak of the probe is in immediate angular proximity to the voided region, which prevents the void from altering the resultant force.
- i) The most eccentric peak is now moving into the angular position of the voided region. The absence of material causes a reduction in the magnitude of the force as the eccentric peak now has less material to push against. *i.e.*, a reduction in the direct contact force.
- j) The most eccentric peak is still in the voided region resulting in a reduced resultant force.
- k) Same condition as in (j)
- 1) The most eccentric peak is now contacting material in the upper right quadrant causing the force to increase back towards its full value of 600 N. The whole process will then repeat itself on the subsequent rotation. Note that a video of the progression shown in Fig. 11 is contained in the Supplementary material.

The fundamental understanding of the probe/defect interaction proposed in Fig. 11 illuminates how aspects of the process will affect the development of a method built on this interaction. The hypothesized interaction relies on the deflection of at least one of the peaks (created by the flats of the tool probe) into a voided volume in the wake of the tool when insufficient material is transferred around the trailing edge of the probe. This deflection leads to a reduction in the contact force between the eccentric peak of the tool probe and the material at the leading edge of the tool probe. This suggests that the design of tool probe features becomes relevant to a detection method based on these transients. For example, a tool probe with deeper flats will create sharper peaks on the tool probe, which may allow for a more significant deflection into a smaller voided volume that produces a larger distortion in the force signals. Tool wear on the probe features can also become relevant to how they interact with void volumes. Additionally, the deflection of the tool suggests that the compliance and dynamics of the machine are relevant, e.g., stiffer machine-tools and tool holder systems will not respond as readily to the presence of a defect as the tool cannot deflect into the voided volume as easily.

Investigations of different aluminum alloys performed by Franke et al. [39] have shown that stronger aluminum alloys result in larger average process forces in the X and Y directions during welding, and thus produce larger amplitudes at the third harmonic for a given defect size. It is hypothesized that the larger average forces create a larger driving force for the deflection of the tool probe into the void volume, resulting in a larger distortion for a given void volume. Future examinations will seek to produce an in situ measurement of the hypothesized tool deflection during defect formation by means of laser

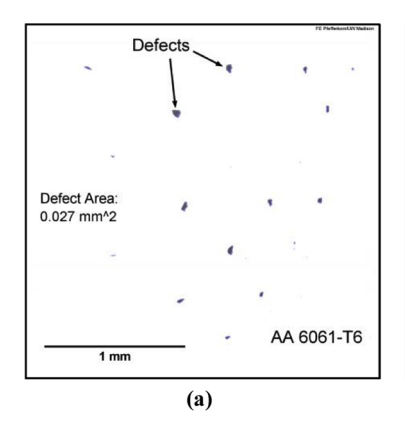
vibrometry. The current hypothesis suggests that it may be possible to sense defect formation through a deflection or acceleration measurement as opposed to a force-based measurement. This would provide the option of attaching an accelerometer to the tool in order to capture significant accelerations at higher harmonic frequencies during void interaction.

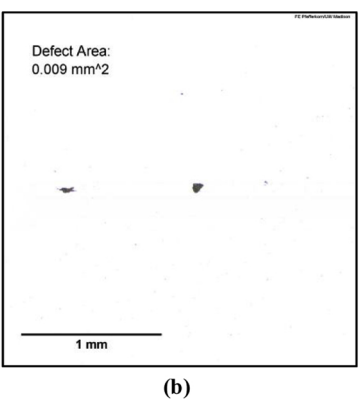
The relationships between the amplitudes of the force transients and the size of the defects generated in the friction stir welds contained in this study will be examined in-depth in a subsequent manuscript. In general, the amplitude of the third harmonic of all three measured force signals (X, Y, and Z) increased with increased defect size. This is consistent with the observations of prior studies [18,34]. However, tool runout and slant are not considered and reported in the prior studies. The runout of the tool must be considered since it is the driver of the workpiece material and probe interaction and thus the generation of the force amplitudes. Additionally, a slant in the tool shoulder has the potential to mask what is occurring at the tool probe(in terms of defect interaction) if it is driving the process force oscillation.

## 3.3. Effect of tool runout on defect formation and size

Welds in a defective process regime were created with all three tools in order to examine how the magnitude of runout affects material flow and defect formation. Interestingly, the tool with the largest runout (Tool 3) started to produce defects at a lower advance per revolution of 0.5 mm/rev as compared to the two tools with lower magnitudes of runout (Tools 1 and 2), which started to form defects at 0.6 mm/rev. In general, defects are more likely to form at conditions of larger advance per revolution because the volume of material that needs to be moved around the tool per revolution becomes larger while the heat input per unit length of weld becomes smaller. Additionally, Tool 3 had much larger measured defect areas as a whole. Tool 3 produced welds with an average defect area of 0.496 mm<sup>2</sup> for all welds performed at the 0.6 mm/rev conditions, while Tools 1 and 2 had average defect areas of 0.010 mm<sup>2</sup> and 0.053 mm<sup>2</sup>, respectively, at the 0.6 mm/rev conditions. When comparing the average defect areas of all the defective welds (0.6 to 0.8 mm/rev conditions) performed with Tool 1 and Tool 2, Tool 2 (74 um runout) had smaller defect sizes with an average defect area of 0.165 mm<sup>2</sup> compared to an average defect area of 0.205 mm<sup>2</sup> for Tool 1 (46 µm runout). An example of the cross sections of defective welds for all three tools performed at the exact same welding conditions of 1000 rpm and 600 mm/min can be observed in Fig. 13. The larger runout of Tool 2 (compared to Tool 1) appeared to help paddle more material around the tool probe per revolution, resulting in smaller defects. However, it appears that Tool 3 had excessive runout that is detrimental to material flow around the tool probe, which resulted in larger defects.

The current results are supported by several prior studies that have shown a larger magnitude of tool eccentricity can help facilitate the flow of material around the tool probe [40–43]. Chen *et al.* [41] showed





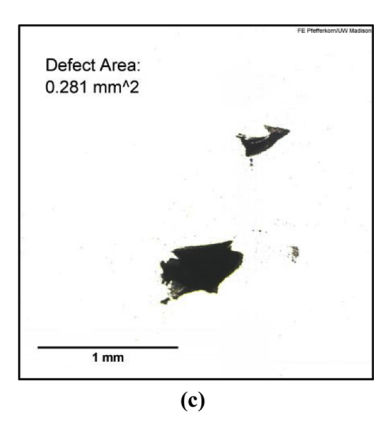


Fig. 13. Images of the defects produced at consistent welding parameters 1000 rpm 600 mm/min by: a Tool 1, b Tool 2, and c Tool 3.

**Table 3**Estimated static compliance of the friction stir welding system utilized in the study.

Direction	Estimated Static Compliance
X	0.51 mm/kN
Y	0.33 mm/kN
Z	0.05 mm/kN [37]

that increased tool eccentricity prevented defect formation and resulted in more distinct onion rings in the weld microstructure. Yuqing et al. [43] determined that indeed material flow increased with increasing tool eccentricity, but only up until a point where the eccentricity becomes too large and reduced material flow. The authors varied the magnitude of tool runout and determined that for a tool with a shoulder diameter of 28 mm and a threaded probe tapering from 10 mm in diameter down to 5 mm in diameter, that a tool runout of 200  $\mu m$ produced a maximum stir zone area (maximum material movement). Tools with runout magnitudes larger than 200 µm resulted in a decreased stir zone size (less material movement). Given that the tools used in the current study (15 mm diameter shoulder) were approximately half the size of the tools used by Yuqing et al., it would be expected that the critical limit for tool runout should be on the order of 100 µm. This concept matches the results of the current study as Tool Number 3 had a runout larger than 100  $\mu m$  and Tools 1 and 2 had runouts less than 100 µm. It is hypothesized that the excessive eccentric motion of the tool probe displaces material from the stir zone radially and vertically rather than stirring it around the tool circumferentially. This displacement of material from the stir zone explains the larger defects observed for Tool 3 as compared to Tools 1 and 2 under similar welding conditions.

## 3.4. Discussion of machine compliance

The results of the current study suggest that the stiffness of the friction stir welding system used to perform the welding is relevant to the generation of the process force transients. Therefore, the compliance of the entire welding system (machine tool, tool holder, tool, workpiece fixture, etc.) was estimated in the X and Y directions in an attempt to increase the transferability of the knowledge contained in this study. This was achieved by loading the tool against the workpiece fixture by incrementing the CNC controller and measuring the applied force to the dynamometer (refer to the Supplementary Material: Section 4 for a full description of compliance determination method). The estimated static compliance of the system is reported in Table 3. The different components of the welding system that contribute to the total system compliance are also described in detail in the Supplementary Material: Section 5. Given that the average process forces measured in the X-direction during defective welds were on the order of 1,000-2,000 N, and Y-direction average forces were on the order of 1,000-3,000 N, substantial deflection of the system is assumed to be achieved. The tool's rotational axis will deflect when the tool is deflected and the tool will now rotate eccentrically around the deflected axis. A tool shoulder that is machined level with respect to the rotational axis will also deflect with the rotational axis and remain level with the respect to the rotational axis. The compliance of the system is also likely to result in the real runout of the tool relative to the workpiece becoming less than the runout value that was measured kinematically for each tool and reported in Table 1, i.e., the forces should have a centering effect on the tool's eccentric motion. Industrial applications of friction stir welding tend to utilize dedicated machine tools that are significantly stiffer than the CNC milling machine used in the current study. Therefore, future studies will examine the nature of force transients during defect formation on larger and stiffer machines. Additionally, the full dynamic characteristics (e.g. mass and damping) may be needed to accurately model the deflection process that occurs during defect interaction. Full dynamic modeling of the system is out of the scope of the current study but may be necessary for future research.

#### 4. Conclusions

A fundamental understanding of the physical mechanisms that drive both process force oscillations and changes in process force transients during defect formation has been proposed. This new understanding allows for a preliminary understanding of how force and torque-based monitoring methods may need to be adapted when altering aspects of the friction stir welding process. It appears that small imperfections from an idealized tool (eccentricity and shoulder slant) drive the oscillatory process forces once per tool revolution, and thus are believed to be fundamental in driving the intermittent flow of material around the tool probe once per tool revolution. During sub-surface defect formation, the peaks of the tool probe created by flats interact with voided volumes during each revolution of the tool resulting in a distortion of the force signal as presented in detail in Section 3.2. This illuminates how process factors should alter the proposed friction stir weld monitoring / detection method. The relevant conclusions from this study can be summarized as follows:

- Larger tool eccentricity drives larger force oscillations, which will alter how the amplitudes at higher harmonics are formed: *i.e.*, tool runout must be considered when developing a monitoring method based on force oscillations and harmonic amplitudes.
- The results suggest that machine compliance/damping and tool design both affect force transients, hence material flow, and must be considered in any process or defect monitoring and detection algorithm.
- Forging position of the trailing shoulder must be considered as the X and Y force distortions only capture an interaction between the voided volume when it is in contact with the tool probe. The voided volume will change in size and shape as the trailing shoulder continues to consolidate the void after it has past the probe.

An additional study will contain the detailed analysis of how the size of defects formed within the friction stir welds produced for this study correlate with a change in process force transients, as well as how a method of defect size prediction can be developed from the force transients. Future studies will also focus on producing *in situ* measurements of the eccentric motion of the tool, as the current study was limited to kinematic measurements of runout. *In situ* measurements will allow for the observation of containment or propagation of the eccentric motion, and tool defection into the voided volume during defect formation. It appears that tool eccentricity is a critical factor, but other factors such as strain localization may need to be considered and modeled.

## **Declaration of Competing Interest**

The authors declare that they have no known competing financial interests or personal relationships that could have appeared to influence the work reported in this paper.

## Acknowledgments

The authors gratefully acknowledge the financial support of this work by the National Science Foundation grant [CMMI-1826104], the Department of Mechanical Engineering at the University of Wisconsin Madison, the Machine Tool Technology Research Foundation, and Friction Stir Link, Inc.

#### Appendix A. Supplementary data

Supplementary material related to this article can be found, in the online version, at doi:https://doi.org/10.1016/j.jmapro.2020.03.003.

#### References

- [1] W.M. Thomas, E.D. Nicholas, J.C. Needham, M.G. Murch, P. Temple-Smith, C.J. Dawes Friction stir butt Welding, 1991. GB Patent No. 9125978.8.
- [2] Mishra RS, Ma ZY. Friction stir welding and processing. Mater Sci Eng R Rep 2005;50:1–78. https://doi.org/10.1016/j.mser.2005.07.001.
- 2005;50:1–78. https://doi.org/10.1016/j.mser.2005.07.001.
   Threadgill PL, Leonard AJ, Shercliff HR, Withers PJ. Friction stir welding of aluminium alloys. Int Mater Rev 2009;54:49–93. https://doi.org/10.1179/174328009X411136
- [4] Tabatabaeipour M, Hettler J, Delrue S, Van Den Abeele K. Nondestructive ultrasonic inspection of friction stir welds. Phys Procedia 2015;70:660–3. https://doi.org/10. 1016/j.phpro.2015.08.071.
- [5] Bird CR. Ultrasonic phased array inspection technology for the evaluation of friction stir welds. Insight - Non-Destructive Test Cond Monit 2004;46(6):31–6. https://doi. org/10.1784/insi.46.1.31.52658.
- [6] Rosado LS, Santos TG, Piedade M, Ramos PM, Vilac AP. Advanced technique for non-destructive testing of friction stir welding of metals. Measurement 2010;43:1021–30. https://doi.org/10.1016/j.measurement.2010.02.006.
- [7] Mandache C, Dubourg L, Merati A, Jahazi M. Pulsed eddy current testing of friction stir welds. Mater Eval 2008;66(4):382–6.
- [8] Qian JW, Li JL, Xiong JT, Zhang FS, Li WY, Lin X. Periodic variation of torque and its relations to interfacial sticking and slipping during friction stir welding. Sci Technol Weld Join 2012;17(4):338–41. https://doi.org/10.1179/1362171812Y. 00000000001.
- [9] Schmidt H, Dickerson TL, Hattel JH. Material flow in butt friction stir welds in AA2024-T3. Acta Mater 2006;54:1199–209. https://doi.org/10.1016/j.actamat. 2005.10.052.
- [10] Abergast WJ. A flow-partitioned deformation zone model for defect formation during friction stir welding. Scr Mater 2008;58:372–6. https://doi.org/10.1016/j. scriptamat.2007.10.031.
- [11] Boldsaikhan E, Burford DA, Gimenez Britos PJ. Effect of plasticized material flow on the tool feedback forces during friction stir welding. In: Mishra R, Murray M, Sato Y, Hovanski Y, Verma R, editors. Friction stir welding and proceeding VI. Wiley; 2011. p. 335–43.
- [12] Nunes AC. Metal flow in friction stir welding. Materials science & technology 2006 conference and exhibition, October 15–19. 2006.
- [13] Fonda R, Reynolds AP, Feng CR, Knipling K, Rowenhorst D. Material flow in friction stir welds. Metall Mater Trans A 2013;44:337–44. https://doi.org/10.1007/s11661-013-1460.6
- [14] Gratecap F, Girard M, Marya S, Racineux G. Exploring material flow in Friction stir welding: tool eccentricity and formation of banded stuctures. Int J Mater Res 2012;5:99–107. https://doi.org/10.1007/s12289-010-1008-5.
- [15] Reynolds AP. Flow visualization and simulation in FSW. Scr Mater 2008;58:338–42. https://doi.org/10.1016/j.scriptamat.2007.10.048.
- [16] Chen ZW, Cui S. On the forming mechanism of banded structures in aluminum alloy friction stir welds. Scr Mater 2008;58:417–20. https://doi.org/10.1016/j. scriptamat.2007.10.026.
- [17] Li WY, Li JF, Zhang ZH, Gao DL, Chao YJ. Metal flow during friction stir welding of 7075-T651 aluminum alloy. Exp Mech 2013;53:1573–82. https://doi.org/10.1007/ s11340-013-9760-3.
- [18] Shrivastava A, Zinn MR, Duffie NA, Ferrier NJ, Smith CB, Pfefferkorn FE. Force measurement-based discontinuity detection during friction stir welding. J Manuf Process 2017;26:113–21. https://doi.org/10.1016/j.jmapro.2017.01.007.
- [19] Balasubramanian N, Mishra R, Krishnamurthy K. Process forces during friction stir channeling in an aluminum alloy. J Mater Process Technol 2011;211:305–11. https://doi.org/10.1016/j.jmatprotec.2010.10.005.
- [20] Balasubramanian N, Gattu B, Mishra RS. Process forces during friction stir welding of aluminium alloys. Sci Technol Weld Join 2009;14(2):141–5. https://doi.org/10. 1179/136217108X372540.
- [21] Ji L, Zuo DW, Wang M. Force response characteristics and mechanical properties of friction stir welded AA2024 sheets. Mater Sci Technol 2016;32(18):1–7. https:// doi.org/10.1080/02670836.2016.1149916.
- [22] Yan JH, Sutton MA, Reynolds AP. Processing and banding in AA2524 and AA2024 friction stir welding. Sci Technol Weld Join 2007;12(5):390–401. https://doi.org/ 10.1179/174329307X213639.

- [23] Boldsaikhan E, McCoy M. Analysis of tool feedback forces and material flow during friction stir welding. In: Mishra R, Mahoney MW, Sato Y, Hovanski Y, Verma R, editors. Friction stir welding and proceeding VII. New Jersey: Wiley; 2013. p. 311–20. Wiley.
- [24] Zaeh MF, Gebhard P. Dynamical behaviour of machine tools during friction stir welding. Prod Eng Res Dev 2010;4:615–24. https://doi.org/10.1007/s11740-010-0273-v.
- [25] Panzer F, Werz M, Welhe S. Experimental investigation of the friction stir welding dynamics of 6000 series aluminum alloys. Prod Eng 2018;12:667–77. https://doi. org/10.1007/s11740-018-0834-z.
- [26] Mishra D, Roy RB, Dutta S, Pal SK, Chakravarty D. A review on sensor based monitoring and control of friction stir welding process and a roadmap to Industry 4.0. J Manuf Process 2018;36:373–97. https://doi.org/10.1016/j.jmapro.2018.10. 016
- [27] Jene T, Dobman G, Wagner G, Eifler D. Monitoring of the friction stir wleding process to describe parameter effects on joint quality. Weld World 2008;52:47–53. https://doi.org/10.1007/BF03266668.
- [28] Fleming P, Lammlein D, Wilkes D, Fleming K, Bloodworth T, Cook G, et al. Inprocess gap detection in friction stir welding. Sens Rev 2008;28(1):62–7. https://doi.org/10.1108/02602280810850044.
- [29] Ramulu PJ, Narayanan RG, Kailas SV, Reddy J. Internal defects and process parameter analysis during friction stir welding of Al 6061 sheets. Int J Adv Manuf Technol 2013;65:1515–28. https://doi.org/10.1007/s00170-012-4276-z.
- [30] Kumar U, Yadav I, Kumari S, Kumari K, Ranjan N, Kesharwani RK, et al. Defect identification in friction stir welding using discrete wavelet analysis. Adv Eng Softw 2015;85:43–50. https://doi.org/10.1016/j.advengsoft.2015.02.001.
- [31] Kumari S, Jain R, Kumar U, Yadav I, Ranjun N, Kumari K, et al. Defect identification in friction stir welding using continuous wavelet transform. J Intell Manuf 2016:1–12. https://doi.org/10.1007/s10845-016-1259-1.
- [32] Das B, Pal S, Bag S. A combined wavelet packet and Hilbert-Huang transform for defect detection and modelling of weld strength in friction stir welding process. J Manuf Process 2016;22:260–8. https://doi.org/10.1016/j.jmapro.2016.04.002.
- [33] Boldsaikhan E, Corwin EM, Logar AM, Arbegast WJ. The use of neural network and discrete Fourier transform for real-time evaluation of friction stir welding. Appl Soft Comput 2011;11:4839–46. https://doi.org/10.1016/j.asoc.2011.06.017.
- [34] Shrivastava A, Pfefferkorn FE, Duffie NA, Ferrier NJ, Smith CB, Malukhin K, et al. Physics-based process model approach for detecting discontinuity during friction stir welding. Int J Adv Manuf Technol 2015;79:604–15. https://doi.org/10.1007/ s00170-015-6868-x.
- [35] D'Orazio A, Forcellese A, Simoncici M. Prediction of the vertical force during FSW of AZ31 magnesium alloy sheets using an artificial neural network-based model. Neural Comput Appl 2019;31:7211–26. https://doi.org/10.1007/s00521-018-3562
- [36] Forcellese A, Martarelli M, Simoncini. Effect of process parameters on vertical forces and temperatures developed during friction stir welding of magnesium alloys. Int J Adv Manuf Technol 2016;85:595–604. https://doi.org/10.1007/s00170-015-7957-6.
- [37] Shultz EF, Cole EG, Smith CB, Zinn MR, Ferrier NJ, Pfefferkorn FE. Effect of compliance and travel angle on friction stir welding with gaps. J Manuf Sci Eng 2010;132:0410101–9.
- [38] Brendel MS, Schneider JA. Long range oscillations in friction stir welding tool travel speed. In: Mishra R, Mahoney M, Sato Y, Hovanski Y, Verma R, editors. Friction stir welding and processing VI. The minerals, metals & materials series. Wiley; 2011. p. 363–71.
- [39] Franke DJ, Zinn MR, Pfefferkorn FE. Intermittent flow of material and force-based defect detection during friction stir welding of aluminum alloys. In: Hovanski Y, Mishra R, Sato Y, Upadhyay P, Yan D, editors. Friction stir welding and processing X. The minerals, metals & materials series. Cham: Springer; 2019. p. 149–60.
- [40] Thomas WM, Nicholas ED. Friction stir welding for the transportation industires. Mater Des 1997;18(4/6):269–73. https://doi.org/10.1016/S0261-3069(97) 00062-9.
- [41] Chen Y, Wang H, Ding H, Zhao J, Zhang F, Ren Z. Influence of tool pin eccentricity on microstructural evolution and mechanical properties of friction stir processed Al-5052 alloy. Mater Sci Eng A 2019;739:272–6. https://doi.org/10.1016/j.msea. 2018.10.057.
- [42] Shah LH, Guo S, Walbridge S, Gerlich A. Effect of tool eccentricity on the properties of friction stir welded AA6061 aluminum alloys. Manuf Lett 2018;15PA:14–7. https://doi.org/10.1016/j.mfglet.2017.12.019.
- [43] Yuquing M, Liming K, Fencheng L, Qiang L, Chunping H, Xing L. Effect of tool pin eccentricity on microstructure and mechanical properties in friction stir welded 7075 aluminum alloy thick plate. Mater Des 2014;62:334–43. https://doi.org/10. 1016/j.matdes.2014.05.038.